Simulation of MHD Flows Using a Hybrid Lattice-Boltzmann Finite-Difference Method

Huayu Li and Hyungson Ki*

Department of Mechanical Engineering, Michigan State University, East Lansing, Michigan 48824-1226, USA.

Abstract. A hybrid lattice-Boltzmann finite-difference method is presented to simulate incompressible, resistive magnetohydrodynamic (MHD) flows. The lattice Boltzmann equation (LBE) with the Lorentz force term is solved to update the flow field while the magnetic induction equation is solved using the finite difference method to calculate the magnetic field. This approach is methodologically intuitive because the governing equations for MHD are solved in their respective original forms. In addition, the extension to 3-*D* is straightforward. For validation purposes, this approach was applied to simulate the Hartmann flow, the Orszag-Tang vortex system (2-*D* and 3-*D*) and the magnetic reconnection driven by doubly periodic coalescence instability. The obtained results agree well with analytical solutions and simulation results available in the literature.

PACS: 47.11.-j, 47.65.-d

Key words: Lattice Boltzmann method, LBM, hybrid, finite difference method, Magnetohydrodynamics, MHD.

1 Introduction

In recent years, the lattice-Boltzmann method (LBM) has experienced enormous success in the simulations of various flow problems [1,2] and attempts have been made to develop LBM algorithms for MHD problems. Chen *et al.* [3] and Martinez *et al.* [4] employed the bidirectional streaming for 2-*D* MHD problems where the distribution function is propagated into two different directions associated with the velocity and magnetic field. The former used 37 discrete velocities while the latter reduced it to 13. Schaffenberger and Hanslmeier [5] later reduced the number of velocities even further to nine by employing the standard streaming rule on a 2-*D* square lattice. Dellar [6] developed a new method, where two distribution functions are utilized to represent the hydrodynamic

---

*Corresponding author. *Email addresses:* `lihuayu@egr.msu.edu` (H. Li), `hski@msu.edu` (H. Ki)

momentum and the magnetic induction. The hydrodynamic part is simulated using the conventional low Mach number LBM, and the magnetic field is represented by a separate vector-valued magnetic distribution function, which obeys the vector Boltzmann-BGK equation. This method has been later extended to 3-*D* by Breyiannis and Valougeorgis [7].

In all the afore-mentioned methods, the magnetic induction problem as well as the flow problem is dealt with by a lattice kinetic approach. While employing LBM for the Boltzmann equation is natural, the use of a kinetic approach for solving the magnetic induction equation is not quite intuitive because, after all, the Boltzmann equation and the magnetic induction equation constitute a set of governing equations for MHD. In other words, a lattice kinetic approach does not need to be used always for the magnetic induction problem even though all-kinetic approaches are more consistent and have many advantages in many cases. In fact, other numerical methods, such as the finite difference method, can be easily employed to solve the magnetic induction equation with equal or better accuracy because those methods are well established.

In this article, the authors present an alternative hybrid method, where the flow field is obtained by LBM and the magnetic induction equation is solved by a finite difference method. Therefore, the fundamental governing equations for MHD are solved without introducing a lattice kinetic approach in the calculation of the magnetic field. This approach can be easily extended to 3-*D*. In this study, this method is applied to Hartmann flow, Orszag-Tang vortex system (both 2-*D* and 3-*D*) and magnetic reconnection problem for validation purposes. The obtained results agree well with analytical solutions and the numerical solutions available in the literature.

2   Mathematical model

The Boltzmann transport equation with the Bhatnagar-Gross-Krook (BGK) collision term is written as:

$$\frac{\partial f}{\partial t} + \xi \cdot \nabla_x f + a \cdot \nabla_\xi f = -\frac{f - f^{eq}}{\lambda}, \tag{2.1}$$

where $f = f(x, \xi, t)$ is the single-particle distribution function in both physical space and phase space, x is the position vector, ξ is the microscopic velocity, a is the acceleration due to the external force exerting on the particles, λ is the relaxation time due to collisions and f^{eq} is the equilibrium distribution function, which is described by the Maxwell-Boltzmann distribution as follows:

$$f^{eq} = \frac{\rho}{(2\pi RT)^{D/2}} exp\left[-\frac{(\xi - u)^2}{2RT}\right], \tag{2.2}$$

where ρ, u, T, R, D are density, macroscopic velocity, temperature, gas constant and dimension of space respectively. For MHD flows, the acceleration a can be written as:

$$a = \frac{1}{\rho\mu}(\nabla \times B) \times B, \tag{2.3}$$

where B is magnetic induction and μ is magnetic permeability. The evolution of magnetic field is obtained by solving the magnetic induction equation, which is derived from Maxwell's equations with the assumption of $\partial E/\partial t = 0$ [8]:

$$\frac{\partial B}{\partial t} = \eta \nabla^2 B + (B \cdot \nabla) u - (u \cdot \nabla) B, \tag{2.4}$$

where η is magnetic diffusivity and is expressed as $\eta = (\mu\sigma)^{-1}$. Here σ is the electrical conductivity. Fluid density and momentum can be retrieved by taking velocity moments of the distribution function as follows:

$$\rho = \int f d\xi, \tag{2.5}$$

$$\rho u = \int \xi f d\xi, \tag{2.6}$$

Eqs. (2.1)-(2.6) form a closed mathematical system that describes the general MHD flows.

In this study, the acceleration term $a \cdot \nabla_\xi f$ in Eq. (2.1) (which couples hydrodynamics and magnetic induction) is evaluated by adopting the following assumption [9]:

$$\nabla_\xi f \approx \nabla_\xi f^{eq} = -\frac{\xi - u}{RT} f^{eq}. \tag{2.7}$$

Then, Eq. (2.1) can be re-written as

$$\frac{\partial f}{\partial t} + \xi \cdot \nabla_x f = -\frac{f - f^{eq}}{\lambda} + \frac{a \cdot (\xi - u)}{RT} f^{eq}. \tag{2.8}$$

The above equation can be discretized as [10]:

$$f_\alpha(x + e_\alpha \triangle t, t + \triangle t) - f_\alpha(x,t) = -\frac{1}{\tau}\left\{f_\alpha(x,t) - \left[1 + 3\tau \triangle t \frac{(e_\alpha - u) \cdot a}{c^2}\right] f_\alpha^{eq}\right\}, \tag{2.9}$$

where τ is the dimensionless relaxation time and e_α is the discrete microscopic velocity. In a $D2Q9$ lattice model, e_α is given as:

$$e_\alpha = \begin{cases} (0,0) & \text{if} \quad \alpha = 0, \\ c\left(\cos\left[\frac{\pi(\alpha - 1)}{2}\right], \sin\left[\frac{\pi(\alpha - 1)}{2}\right]\right) & \text{if} \quad \alpha = 1,2,3,4, \\ \sqrt{2}c\left(\cos\left[\frac{\pi(\alpha - 5)}{2} + \frac{\pi}{4}\right], \sin\left[\frac{\pi(\alpha - 5)}{2} + \frac{\pi}{4}\right]\right) & \text{if} \quad \alpha = 5,6,7,8. \end{cases} \tag{2.10}$$

The discretized equilibrium distribution function under the low Mach number assumption is:

$$f_\alpha^{eq} = \omega_\alpha \rho \left[1 + \frac{3(e_\alpha \cdot u)}{c^2} + \frac{9(e_\alpha \cdot u)^2}{2c^4} - \frac{3u^2}{2c^2}\right]. \tag{2.11}$$

In Eq. (2.11) , the coefficient ω_α is 4/9 for $\alpha = 0$, 1/9 for $\alpha = 1:4$, and 1/36 for $\alpha = 5:8$. $c = \triangle x / \triangle t$, where $\triangle x$ is the lattice spacing and $\triangle t$ is the time step. The particle distribution function is updated by Eq. (2.9) through the standard streaming step and collision step [11]. The macroscopic density and momentum can be retrieved by:

$$\rho = \sum_\alpha f_\alpha, \tag{2.12}$$

$$\rho u = \sum_\alpha e_\alpha f_\alpha. \tag{2.13}$$

The magnetic induction equation (Eq. (2.4)) is solved by the conventional finite difference method. In two dimensions, for example, the $x-$component of Eq. (2.4) is written as:

$$\frac{\partial B_x}{\partial t} = \frac{1}{\mu\sigma} \left(\frac{\partial^2 B_x}{\partial x^2} + \frac{\partial^2 B_x}{\partial y^2} \right) + B_x \frac{\partial u_x}{\partial x} + B_y \frac{\partial u_x}{\partial y} - u_x \frac{\partial B_x}{\partial x} - u_y \frac{\partial B_x}{\partial y}. \tag{2.14}$$

The following discretized equation is obtained if the central difference scheme is employed:

$$\begin{aligned}
\frac{\partial (B_x)_{i,j}}{\partial t} = \frac{1}{\mu\sigma} & \left[\frac{(B_x)^n_{i+1,j} - 2(B_x)^n_{i,j} + (B_x)^n_{i-1,j}}{(\triangle x)^2} + \frac{(B_x)^n_{i,j+1} - 2(B_x)^n_{i,j} + (B_x)^n_{i,j-1}}{(\triangle y)^2} \right] \\
& + (B_x)^n_{i,j} \frac{(u_x)^n_{i+1,j} - (u_x)^n_{i-1,j}}{2\triangle x} + (B_y)^n_{i,j} \frac{(u_x)^n_{i+1,j} - (u_x)^n_{i,j-1}}{2\triangle y} \\
& - (u_x)^n_{i,j} \frac{(B_x)^n_{i+1,j} - (B_x)^n_{i-1,j}}{2\triangle x} - (u_y)^n_{i,j} \frac{(B_x)^n_{i,j+1} - (B_x)^n_{i,j-1}}{2\triangle y}. \tag{2.15}
\end{aligned}$$

Note that all the terms on the right hand side are evaluated at time step n using the fluid velocity calculated by the lattice Boltzmann solver. Eq. (2.15) can be re-written as follows:

$$\frac{\partial (B_x)_{i,j}}{\partial t} = R((B_x)^n). \tag{2.16}$$

In this study, the time derivative on the left hand side is discretized by the second-order Runge-Kutta method:

$$\begin{aligned}
(B_x)^{n+1/2} &= (B_x)^n + \frac{\triangle t}{2} R((B_x)^n), \\
(B_x)^{n+1} &= (B_x)^n + \triangle t R\left((B_x)^{n+1/2} \right). \tag{2.17}
\end{aligned}$$

3 Numerical tests

3.1 Hartmann flow

For validation purposes, the 2-*D* Hartmann flow is simulated because its analytical solution can be easily obtained. Hartman flow is a channel flow induced by a uniform

magnetic field(B_0) applied perpendicular to the flow direction. For 2-D Hartmann flows, velocity has only one component in the channel direction $u = (u_x, 0, 0)$ and this flow induces additional magnetic field in the flow direction. Therefore, magnetic field can be written as $B = (B_x, B_0, 0)$. The magnetic induction equation and the hydrodynamic momentum equation can be simplified as follows:

$$\frac{1}{\mu\sigma}\frac{d^2 B_x}{dy^2} + B_0\frac{du_x}{dy} = 0, \tag{3.1}$$

$$\rho v\frac{d^2 u_x}{dy^2} + \frac{B_0}{\mu}\frac{dB_x}{dy} = g, \tag{3.2}$$

where v is kinematic viscosity and $g = dp/dx$ is the constant pressure gradient used to drive the flow along the $x-$direction. By using the following boundary conditions

$$\begin{cases} u_x = 0 & at \quad y = \pm L, \\ B_x = 0 & at \quad y = \pm L, \end{cases} \tag{3.3}$$

the analytical solutions to Eqs. (3.1) and (3.2) are obtained as:

$$u_x(y) = \frac{gM}{\sigma B_0^2}\coth(M)\left[\frac{\cosh(My/L)}{\cosh(M)} - 1\right], \tag{3.4}$$

$$B_x(y) = -\frac{g\mu L}{B_0}\left[\frac{\sinh(My/L)}{\sinh(M)} - \frac{y}{L}\right], \tag{3.5}$$

where $M = B_0 L\sqrt{\sigma/\rho v}$ is the Hartmann number. If there is no external magnetic field, the Hartmann number becomes zero and the flow reduces to the Poiseuille flow, which has solutions of $u_x(y) = g(L^2 - y^2)/2\rho v$ and $B_x = 0$.

For the LBM simulation of the Hartmann flow, the initial distribution function is set to the equilibrium distribution function with constant density, $\rho = 1.0$, u_x and B_x are set to zero. A uniform magnetic field B_0 is applied in the $y-$direction. The bounce-back condition is used for wall boundaries while the periodic boundary condition is used at the inlet and the outlet [12]. The simulation is terminated when a steady state is reached. To drive the flow, the driving pressure gx is added to the external force as follows:

$$\rho a = J \times B + g\hat{e}_x, \tag{3.6}$$

where $\hat{e}_x$ is the unit vector in the $x-$direction.

Figs. 1 and 2 present simulation results of u_x and B_x respectively, where solid lines denote analytical solutions given by Eqs. (3.4) and (3.5). As clearly seen, the simulation results agree well with the analytical solutions for all Hartmann numbers considered. In this simulation, a 200×20 grid is used and the parameters of $\tau = 0.635$, $\sigma = 10$ and $g = 2.5\times 10^{-5}$ are adopted. The Hartmann numbers of 0, 1, 2, 5, 10 and 20 are considered. Note that the Hartmann number can be changed by varying the magnitude of the applied magnetic
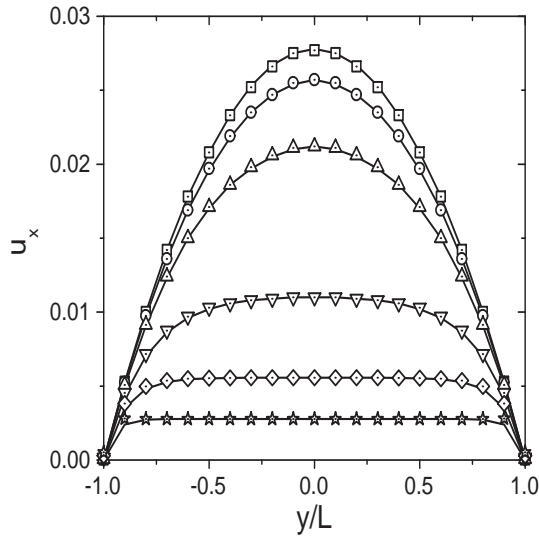
Figure 1: Velocity profiles for different Hartmann numbers: $M=0$ (squares), $M=1$ (circles), $M=2$ (upper triangles), $M=5$ (lower triangles), $M=10$ (diamonds), $M=20$ (stars). The solid lines show the analytical solutions.
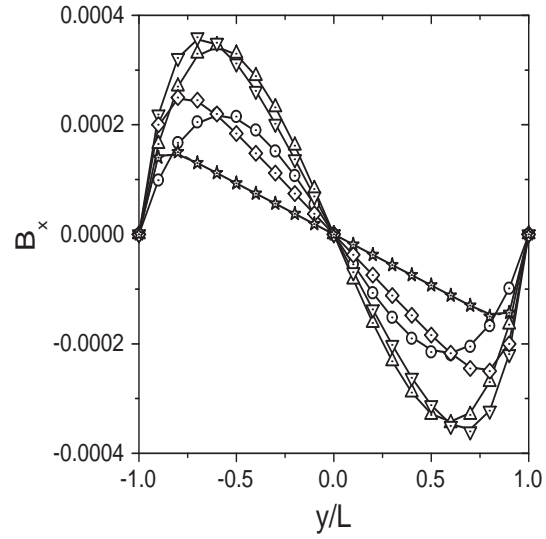
Figure 2: Profiles of $x-$component magnetic field for different Hartmann numbers: $M=1$ (circles), $M=2$ (upper triangles), $M=5$ (lower triangles), $M=10$ (diamonds), $M=20$ (stars). The solid lines show the analytical solutions.

field B_0. In Fig. 1, it is shown that as the Hartmann number increases the velocity profile becomes flatter, which can be explained by Eq. (3.4). Clearly, the applied magnetic field (B_0) tends to reduce the magnitude of $x-$component velocity. If the Hartmann number is finite, the velocity profile cannot be entirely flat even for very large Hartmann numbers and there must be a region with a large velocity gradient because velocity is forced to be zero due to the no slip boundary conditions. Fig. 2 presents the magnetic field induced by the flow for a variety of Hartmann numbers, the simulation results agree with the analytical solutions very well.

3.2 Orszag-Tang vortex

As the second test problem, the Orszag-Tang vortex system (which is an unsteady, non-linear MHD flow problem) was chosen. Since Orszag and Tang [13] first studied this problem, it has become a popular benchmark problem because many aspects of MHD turbulent flows appear in this problem, such as the dynamic alignment, selective decay and magnetic reconnection [14]. In this study, a 2-D Orszag-Tang vortex problem is simulated with the following simple nonrandom deterministic initial conditions:

$$u_0 = -u_0(\sin y, -\sin x),$$
$$B_0 = -B_0(\sin y, -\sin(2x)), \tag{3.7}$$

where $u_0 = 2.0$ and $B_0 = 2.0$ are the initial velocity and magnetic induction, respectively. The simulation is performed on a square domain of $0 \le x, y \le 2\pi$. A 512×512 uniform grid is used and the periodic boundary conditions are applied on all boundaries. Kinematic fluid viscosity and magnetic diffusivity are assumed to be the same ($v = \eta = 0.02$), which leads to the same Reynolds number (Re) and magnetic Reynolds number (Re_m) at the initial stage. With the initial conditions shown in Eq. (3.7), the evolution of the vorticity of fluid ($\omega = \nabla \times u$) and the current density ($j = \nabla \times B / \mu_0$) are demonstrated in Figs. 3 and 4, respectively. As shown in Figs. 3 and 4, initially both velocity field and magnetic field have symmetric structures. As time elapses, the initial flow pattern becomes complicated due to the nonlinear interactions between the velocity field and the magnetic field. In Fig. 4, the existing current sheet at the center of the figure is enhanced and eventually, a thin elliptic structure establishes due to the magnetic reconnection occurring there. At the same time, a region of sheared flow coexists with the current sheet, which is shown as the flat quadrupole-like configuration in Fig. 3. The contours of the vorticity and the current density agree well qualitatively with the simulation results available in the literature [14].
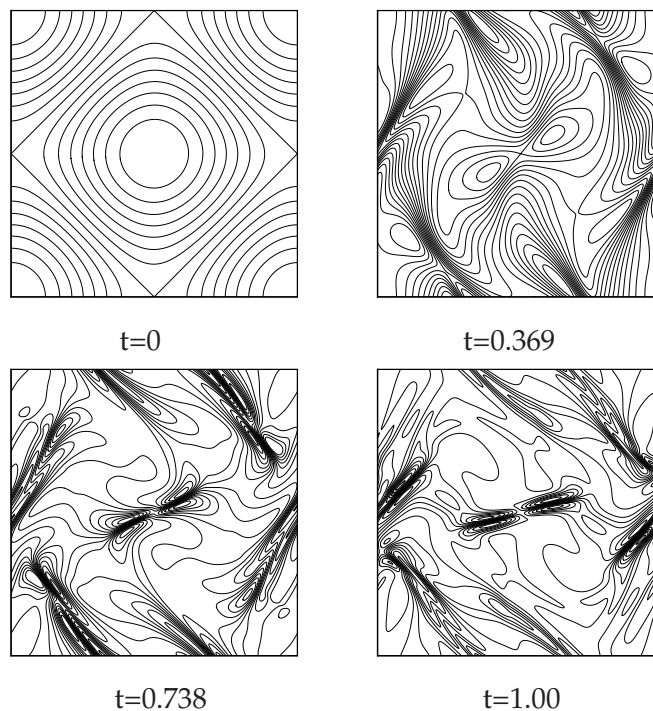

t=0   t=0.369

t=0.738   t=1.00

Figure 3: Evolution of vorticity for the 2-D Orszag-Tang vortex (time in sec).

In order to validate this model quantitatively, this problem was simulated by using the same parameters used in the paper by Dellar [6] ($u_0 = 2.0, v = \eta = 0.02$, and a 512×512 grid).The maximum vorticity value at $t = 0.5$ sec predicted by this model is 6.764 while Dellar's result gives a values of 6.758. At $t = 1.0$ sec, the values are 14.457 and 14.20
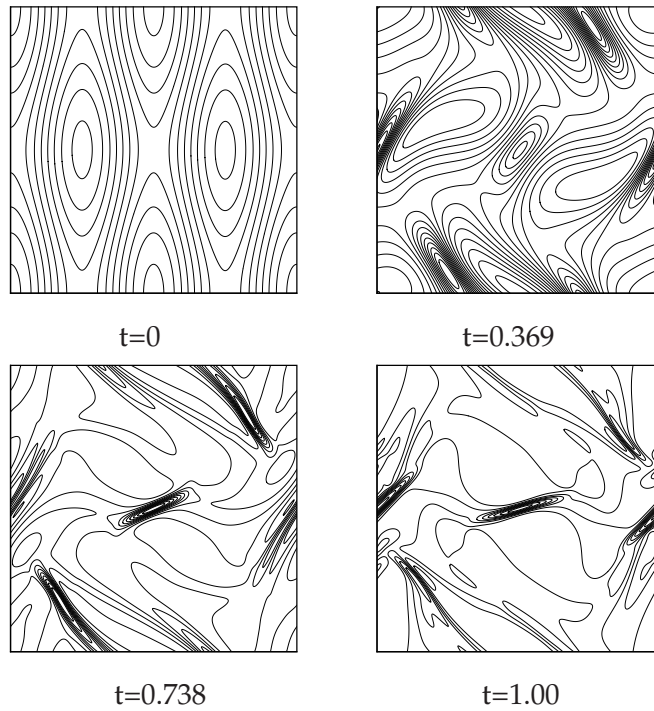
t=0   t=0.369

t=0.738   t=1.00

Figure 4: Evolution of current density for the 2-*D* Orszag-Tang vortex (time in sec).

Table 1: Quantitative comparison of simulation results with Dellar's work.

	Time(sec)	Max vorticity	Max current	$|\nabla \cdot B|$
Present results	0.50	6.764	18.129	0.00463
	1.0	14.457	45.963	0.00922
Dellar's results	0.50	6.758	18.24	0.0062
	1.0	14.20	46.59	0.0415

respectively. The maximum current densities are also compared and the values are given in Table 1. In order to check if these two models satisfy the divergence-free property of the magnetic field, the values of $|\nabla \cdot B|$ are calculated. The presented model gives 0.00463 at $t = 0.5$ sec and 0.00922 at $t = 1.0$ sec while Dellar's results indicate 0.0062 and 0.0415 at the corresponding times. Therefore, the presented model is validated quantitatively, too.
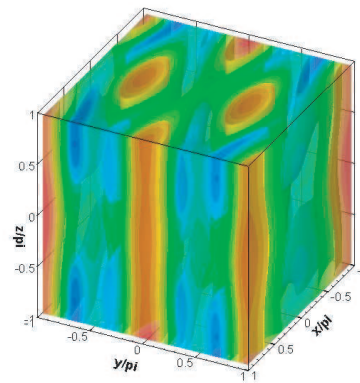
To show that this model can be easily extended to 3-*D*, the D3Q19 lattice model [15] has been employed to solve the 3-*D* Orszag-Tang vortex problem with the following initial conditions [16]:

$$
\begin{aligned}
u_0 &= (-2\sin y, 2\sin x, 0), \\
B_0 &= 0.8(-2\sin(2y) + \sin z, 2\sin x + \sin z, \sin x + \sin y).
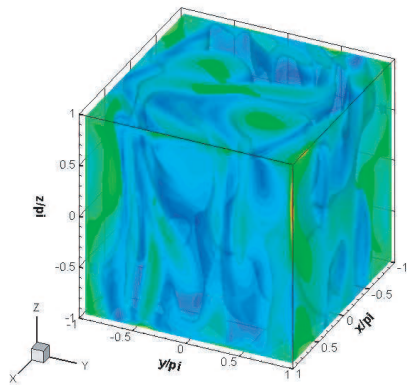\end{aligned}
\tag{3.8}
$$

A cubic domain of $2\pi \times 2\pi \times 2\pi$ is used and simulations are conducted on a $64 \times 64 \times 64$
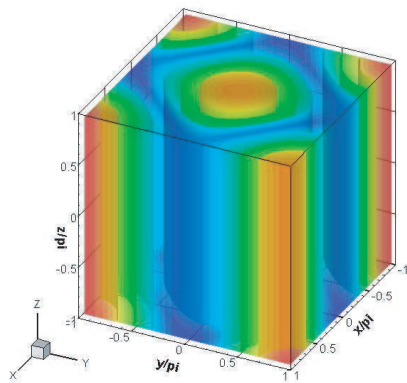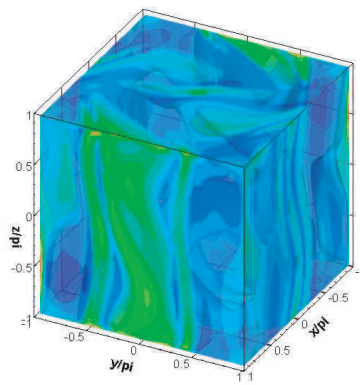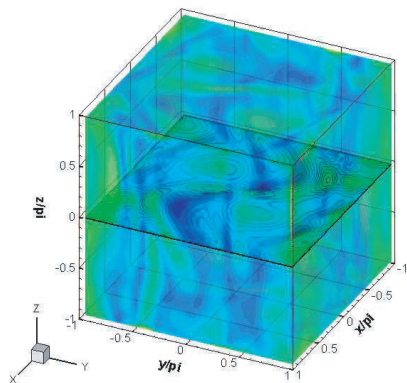
(a) $|\omega|$ at t=0 sec

(b) $|j|$ at t=0 sec

(c) $|\omega|$ at t=0.598 sec

(d) $|j|$ at t=0.598 sec

(e) $|\omega|$ at t=0.598 sec with a 2D contour at z=0. (f) $|j|$ at t=0.598 sec with a 2D contour at z=0.

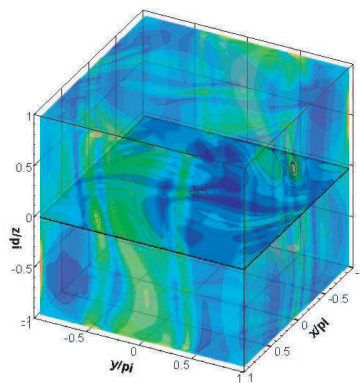Figure 5: Iso-surface contours of magnitudes of vorticity and current density at $t=0$ and $t=0.598$ sec for the 3-D Orszag-Tang vortex.

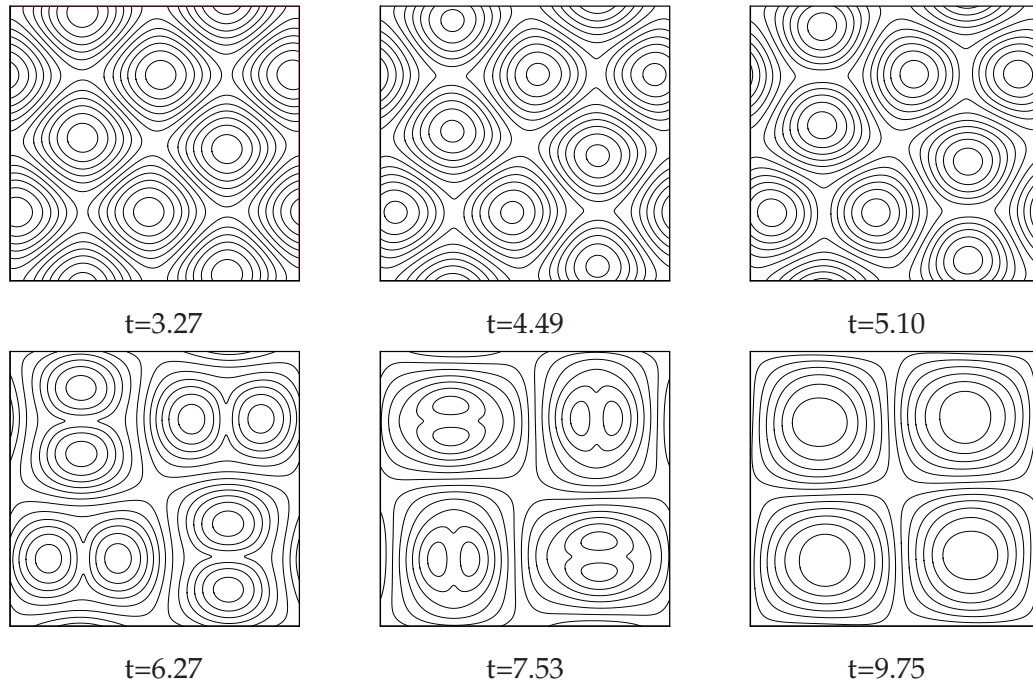| t=3.27 | t=4.49 | t=5.10 |

| t=6.27 | t=7.53 | t=9.75 |

Figure 6: Evolution of magnetic flux function for doubly periodic coalescence instability (time in sec).

grid. Periodic boundary conditions are used for all boundary surfaces and edges. Fig. 5a-5b shows the initial contours of the magnitudes of vorticity ($|\omega|$) and current density $|j|$ and Fig. 5c-5d are the same plots at $t = 0.598$ sec. To investigate the emergence of the sheered current density and flow, the 2-D contours of $|\omega|$ and $|j|$ at $z = 0$ and $t = 0.598$ sec are presented in Fig. 5e-5f. The patterns of the current sheet and the corresponding vorticity resemble Figs. 3 and 4 closely because initially current density and vorticity in $x-$ and $y-$directions are relatively smaller in values than those in the $z-$direction.

3.3   Magnetic reconnection driven by doubly periodic coalescence instability

Magnetic reconnection is the process where magnetic field lines from different magnetic domains merge into one another, changing the overall topology of the magnetic field. Meanwhile, the stored magnetic energy is released in heat and kinetic energy forms. The magnetic reconnection can be driven by different forms of coalescence instability, for example, by the merging of a chain of magnetic islands [17] or by doubly periodic coalescence instability [18]. In this study, a magnetic reconnection problem driven by the doubly periodic coalescence instability is simulated using the present model. As the initial distribution of magnetic flux, a checkerboard pattern [19] represented by Eq. (3.9) is employed.

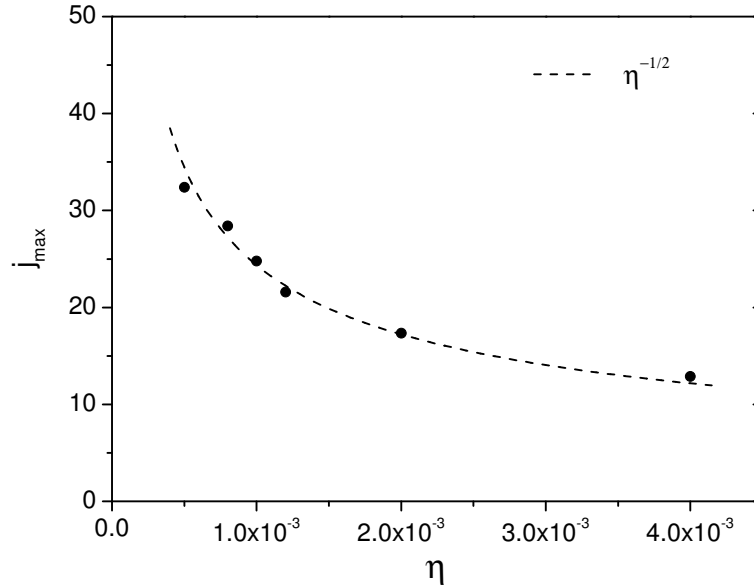$$\psi_0(x,y) = B_0 \sin(\pi(x+y))\sin(\pi(x-y)). \tag{3.9}$$

Figure 7: Maximum value of current density vs. magnetic diffusivity.

The symmetric initial perturbation of the kinetic stream function is:

$$\varphi_0(x,y) = u_0 \exp(-10(x^2 + y^2)), \tag{3.10}$$

where $B_0 = 0.5/\pi$, $u_0 = 0.05$ and the initial magnetic and velocity fields are obtained as follows:

$$B_0 = \hat{e}_z \times \nabla \psi_0 = \left(-\frac{\partial \psi_0}{\partial y}, \frac{\partial \psi_0}{\partial x}\right),$$

$$u_0 = \hat{e}_z \times \nabla \varphi_0 = \left(-\frac{\partial \varphi_0}{\partial y}, \frac{\partial \varphi_0}{\partial x}\right). \tag{3.11}$$

The simulation is conducted on a square domain of $-1 \leq x$, $y \leq 1$ and a 256×256 grid is used. Periodic boundary conditions are used on all boundaries. A fixed viscosity of $v = 4 \times 10^{-3}$ is used; five values of magnetic diffusivity ($\eta = 0.5 \times 10^{-3}$, 0.8×10^{-3}, 1×10^{-3}, 2×10^{-3} and 4×10^{-3}) are considered. Fig. 6 presents the evolution of magnetic flux at different times with the magnetic diffusivity of 1×10^{-3}. Note that the position of the magnetic current sheets does not change with time because the initial perturbation of the kinetic stream function has a mirror symmetry with respect to x and y directions. It can be seen from Fig. 6 that the magnetic islands with currents of the same sign move towards each other. The two corners coalesce into one and the original two square cells become two adjacent pentagons. A current sheet forms between the two cells and the intensity of the current sheet increases. Eventually, the neighboring square cells merge together, simplifying the topology structure of the magnetic field to four square-like islands. Fig. 7,

presenting the dependence of maximum current density on magnetic diffusivity, is a quantitative evidence of the present model. As seen from the plot, the temporal maximum of current density can be approximated as $j_{max} \propto \eta^{-1/2}$ as illustrated by the dashed line in Fig. 7, which can be compared with Fig. 3 in [19].

4 Conclusion

In this article, a lattice Boltzmann method for incompressible, resistive MHD flows is presented. The hydrodynamic part was calculated by LBM and the magnetic induction equation was solved by the finite difference method. Its implementation is relatively simple compared to other LBMs and Navier-Stokes equation based methods. In addition, the extension to 3-D is straightforward. The authors believe that this approach is a good alternative to other MHD-LBMs that are fully based on the lattice kinetic algorithms. Three classic problems in MHD flows were solved in this study and the obtained results agreed well with the data available in the literature.

Acknowledgments

References

[1] Karlin, I.V., S. Ansumali, C.E. Frouzakis and S.S. Chikatamarla, Elements of the lattice Boltzmann method I: Linear advection equation, Commun. Comput. Phys., 1(4)(2006), 616-655.

[2] Karlin, I.V., S.S. Chikatamarla and S. Ansumali, Elements of the lattice Boltzmann method II: Kinetics and hydrodynamics in one dimension, Commun. Comput. Phys., 2(2)(2007), 196-238.

[3] Chen, S.Y., H.D. Chen, D. Martinez and W. Matthaeus, Lattice Boltzmann model for simulation of magnetohydrodynamics, Phys. Rev. Lett., 67(27)(1991), 3776-3779.

[4] Martinez, D.O., S.Y. Chen and W.H. Matthaeus, Lattice Boltzmann magnetohydrodynamics, Phys. Plasmas, 1(6)(1994), 1850-1867.

[5] Schaffenberger, W. and A. Hanslmeier, Two-dimensional lattice Boltzmann model for magnetohydrodynamics, Phys. Rev. E, 66(4)(2002), 046702.

[6] Dellar,P.J., Lattice kinetic schemes for magnetohydrodynamics, J. Comput. Phys., 179(1) (2002), 95-126.

[7] Breyiannis, G. and D. Valougeorgis, Lattice kinetic simulations in three-dimensional magnetohydrodynamics, Phys. Rev. E, 69(6)(2004), 065702.

[8] Bittencourt, J.A., Fundamentals of Plasma Physics. 3rd ed. 2004, New York: Springer. xxiii, 678.

[9] He, X.Y., X.W. Shan and G.D. Doolen, Discrete Boltzmann equation model for nonideal gases, Phys. Rev. E, 57(1)(1998), R13-R16.

[10] He, X.Y. and L.S. Luo, Theory of the lattice Boltzmann method: From the Boltzmann equation to the lattice Boltzmann equation, Phys. Rev. E, 56(6)(1997), 6811-6817.

[11] Chen, S. and G.D. Doolen, Lattice Boltzmann method for fluid flows, Annual Review of Fluid Mechanics, 30(1998), 329-364.

[12] Succi, S., The lattice Boltzmann equation for fluid dynamics and beyond. Numerical Mathematics and Scientific Computation. 2001, Oxford. New York: Clarendon Press; Oxford University Press. xvi, 288.

[13] Orszag, S.A. and C.M. Tang, Small-scale structure of 2-dimensional magnetohydrodynamic turbulence, J. Fluid Mech., 90(JAN)(1979), 129-143.

[14] Dahlburg, R.B. and J.M. Picone, Evolution of the Orszag-Tang vortex system in a compressible medium. 1. Initial average subsonic flow. Physics of Fluids B-Plasma Physics, 1(11)(1989), 2153-2171.

[15] Mei, R., W. Shyy, D. Yu and L. Luo, Lattice Boltzmann method for 3-D flows with curved boundary, J. Comput. Phys., 161(2)(2000), 680-699.

[16] Grauer, R. and C. Marliani, Current-sheet formation in 3D ideal incompressible magnetohydrodynamics, Phys. Rev. Lett., 84(21)(2000), 4850-4853.

[17] Finn, J.M. and P.K. Kaw, Coalescence instability of magnetic islands, Phys. Fluids, 20(1)(1977), 72-78.

[18] Longcope, D.W. and H.R. Strauss, The coalescence instability and the development of current sheets in 2-dimensional magnetohydrodynamics, Physics of Fluids B-Plasma Physics, 5(8)(1993), 2858-2869.

[19] Marliani, C. and H.R. Strauss, Reconnection of coalescing magnetic islands, Phys. Plasmas, 6(2)(1999), 495.